Spontaneous Localization from Cosmological Geometry: A Parameter-Free Derivation of the Collapse Kernel, Thermodynamic Viability, and Falsifiable Cosmological Signature

Brian C. Nyberg[1, *]

[1] *Independent Researcher, Cedar City, Utah, USA*

(Dated: April 9, 2026)

We propose that the objective collapse of the quantum wavefunction is not a phenomenological addition to quantum mechanics, but a strict geometric necessity driven by macroscopic cosmological expansion. Working within a strictly real-valued quantum framework governed by a J-balanced quotient space, we first prove that local tomography is exactly restored without recourse to the complex field $\mathbb{C}$ (Theorem I). By treating the unobserved universal environment as a high-dimensional spherical embedding, measure concentration rigorously derives the localized spatial density matrix, replacing the arbitrary Gaussian parameter of standard collapse models (GRW, CSL) with the fundamental geometric soft-edge σ (Theorem II). Evaluating the continuous momentum injection reveals a violent σ^{-5} ultraviolet divergence. We prove that balancing this microscopic heating against the macroscopic cosmological Ricci scalar tension $\lambda_{\text{geo}} = \omega_P|\mathcal{R}_{\text{dim}}|$ mathematically forces a critical localization scale of $\sigma_{\text{crit}} \approx 3.7 \times 10^{-13}$ meters—the electron Compton wavelength—satisfying LISA Pathfinder bounds with zero free parameters in the microscopic collapse dynamics (Theorem III). Integrating this geometrically triggered friction into the perturbed Einstein–Boltzmann equations predicts a non-degenerate, chirped residual in the matter power spectrum, with onset at redshift $z \approx 24$ coinciding with the epoch of Cosmic Dawn (Theorem IV). Confrontation with DESI DR1 baryon acoustic oscillation measurements yields $\Delta\chi^2 = 4.28$ improvement over standard ΛCDM with a single effective coupling parameter, providing suggestive evidence that large-scale structure anomalies may constitute the macroscopic footprint of quantum wavepacket collapse.

I. INTRODUCTION

The measurement problem remains the central unresolved question in the foundations of quantum mechanics. While the formalism of unitary evolution under the Schrödinger equation is universally accepted, the mechanism by which definite measurement outcomes emerge from superposition states has resisted consensus for nearly a century.

Objective collapse models—most prominently the Ghirardi–Rimini–Weber (GRW) theory [1] and Continuous Spontaneous Localization (CSL) [2, 3]—propose that wavefunction collapse is a real physical process governed by a stochastic, nonlinear modification of the Schrödinger equation. These models introduce a spatial localization operator, universally taken to be a Gaussian kernel $\exp\left[-\lambda_c(x-y)^2\right]$, which continuously narrows the position-space wavepacket.

Despite their elegance, these models suffer from two critical vulnerabilities:

1. **The parameter problem.** The Gaussian smearing parameter σ and the collapse rate λ are phenomenological—inserted by hand to match macroscopic definiteness without violating microscopic interference. They lack derivation from deeper principles.

2. **The heating problem.** Continuous spatial localization injects momentum via the Heisenberg uncertainty principle ($\Delta x \downarrow \Rightarrow \Delta p \uparrow$), producing anomalous energy gain $\dot{E} > 0$. Standard white-noise CSL models predict heating rates increasingly constrained by precision experiments including LISA Pathfinder [4] and ultracold cantilevers [5].

In this work, we resolve both vulnerabilities simultaneously by deriving the collapse kernel and its rate from cosmological geometry, with zero free parameters in the microscopic collapse dynamics. We refer to this framework as the *Three-Body Architecture*, reflecting the irreducible triad of the local quantum subsystem, the high-dimensional environmental manifold, and the macroscopic cosmological background whose interplay generates the collapse. The argument proceeds in four stages:

Section II establishes the kinematic foundation. Working entirely within real vector spaces equipped with an antisymmetric complex structure J, we construct a J-balanced quotient composition law that exactly restores local tomography, bypassing the Wootters–Hardy no-go theorems [6, 7] for real quantum mechanics. The Born rule is derived via the Busch–Gleason route [8] on the unsharp effect algebra, requiring neither $\mathbb{C}$ nor the dimensional restriction $d \geq 3$ of the original Gleason theorem [9].

Section III derives the collapse kernel. By modeling the unobserved environment on a high-dimensional hypersphere and applying Lévy's lemma of measure concentration [10, 11], we prove that the physical shadow map—the CPTP partial trace over the environment—converges to the exact Gaussian spatial decoherence functional in

* docnyberg@gmail.com

the thermodynamic limit. The arbitrary parameter σ is thereby eliminated, reidentified as the metric variance of the underlying manifold.

Section IV confronts the heating problem. The momentum-space correlator derived from the geometric kernel produces a σ^{-5} ultraviolet divergence. We prove that coupling the collapse rate to the contemporary cosmological Ricci scalar $\lambda_{\rm geo} = \omega_P|\mathcal{R}_{\rm dim}|$ yields exact thermodynamic balance, forcing $\sigma_{\rm crit} \approx 3.7 \times 10^{-13}$ m—the electron Compton wavelength—without phenomenological adjustment.

Section V derives the observable consequence. Integrating the geometrically thresholded friction into the perturbed Einstein–Boltzmann equations generates a chirped residual in the matter power spectrum with onset at $z \approx 24$, coinciding with Cosmic Dawn. This nondegenerate signature is falsifiable against DESI and future spectroscopic surveys.

II. THE KINEMATIC QUOTIENT: RESTORING LOCAL TOMOGRAPHY IN REAL VECTOR SPACES

A. Algebraic foundations

We strip the *a priori* axiomatic privilege of the complex field $\mathbb{C}$ and replace it with real geometry constrained by a continuous symmetry.

Definition II.1 (Local kinematic space)**.** Let a local physical system be described by a finite-dimensional real inner-product space $V \cong \mathbb{R}^{2d}$ equipped with a positive-definite metric $g(\cdot,\cdot)$ and a complex structure $J \in \mathrm{SO}(2d)$ satisfying

$$J^2 = -I_{2d}, \qquad g(Jx, Jy) = g(x, y) \implies J^T = -J. \quad (1)$$

Definition II.2 (J-compatible observable algebra)**.** The bounded observables $\mathcal{O}_J(V)$ are the symmetric endomorphisms that strictly commute with the complex structure:

$$\mathcal{O}_J(V) = \{A \in \mathrm{End}(V) \mid A = A^T,\ [A, J] = 0\}. \quad (2)$$

Lemma II.3 (Local dimension bound)**.** *The real dimension of the local observable algebra is exactly* $\dim_{\mathbb{R}}(\mathcal{O}_J(V)) = d^2$.

Proof. In the Darboux-canonical basis where $J = \left(\begin{smallmatrix} 0 & -I_d \\ I_d & 0 \end{smallmatrix}\right)$, any $A \in \mathcal{O}_J(V)$ takes the block form $A = \left(\begin{smallmatrix} X & -Y \\ Y & X \end{smallmatrix}\right)$. The symmetry condition $A = A^T$ imposes $X = X^T$ (symmetric, $\frac{1}{2}d(d+1)$ parameters) and $Y = -Y^T$ (antisymmetric, $\frac{1}{2}d(d-1)$ parameters). The total is

$$\dim_{\mathbb{R}}(\mathcal{O}_J(V)) = \tfrac{1}{2}d(d+1) + \tfrac{1}{2}d(d-1) = d^2. \quad (3)$$

This exactly recovers the parameter count of a complex Hermitian matrix of dimension d, derived entirely from real matrix geometry. □

B. The J-balanced composition law

Lemma II.4 (RQM tomographic deficit)**.** *In standard real quantum mechanics, the bipartite state space $V_A \otimes_{\mathbb{R}} V_B$ has real dimension $(2d_A)(2d_B) = 4d_Ad_B$. The joint observable algebra on this raw tensor product has dimension $\frac{1}{2}(4d_Ad_B)(4d_Ad_B + 1)$, which strictly exceeds the product of local observable dimensions $d_A^2 \cdot d_B^2$. This introduces non-local hidden degrees of freedom, breaking local tomography.*

Definition II.5 (J-synchronization ideal)**.** The algebraic ideal $\mathcal{I}_J \subset V_A \otimes_{\mathbb{R}} V_B$ is generated by the redundant relative symmetries between the two local complex structures:

$$\mathcal{I}_J = \mathrm{span}_{\mathbb{R}}\{(J_Ax \otimes y) - (x \otimes J_By) \mid x \in V_A,\ y \in V_B\}. \quad (4)$$

Definition II.6 (J-balanced bipartite space)**.** The joint physical state space is the quotient:

$$V_{AB} = (V_A \otimes_{\mathbb{R}} V_B)/\mathcal{I}_J. \quad (5)$$

Theorem II.7 (Restoration of local tomography)**.** *The J-balanced state space V_{AB} permits strict local tomography: a joint state is uniquely and completely determined by local measurements.*

Proof. (i) Dimension halving. The quotient condition enforces $J_Ax \otimes y \equiv x \otimes J_By$, mandating $J_A \otimes I_B \sim I_A \otimes J_B$. Because $J^2 = -I$, this pairing exactly halves the raw tensor degrees of freedom:

$$\dim_{\mathbb{R}}(V_{AB}) = \tfrac{1}{2}(4d_Ad_B) = 2d_Ad_B. \quad (6)$$

(ii) Global structure. The quotient inherits a well-defined joint complex structure J_{AB} acting on equivalence classes as $J_{AB}[x \otimes y] = [J_Ax \otimes y] = [x \otimes J_By]$.

(iii) Joint observable dimension. By Definition II.2 and Lemma II.3, substituting the effective subsystem dimension $D = d_Ad_B$:

$$\dim_{\mathbb{R}}(\mathcal{O}_J(V_{AB})) = D^2 = (d_Ad_B)^2 = d_A^2\, d_B^2. \quad (7)$$

The joint observable dimension exactly equals the product of local dimensions, exhausting the parameter space by local product measurements alone. There is no Wootters–Hardy dimensional excess. □

Remark. For the qubit case $d = 2$: the raw real tensor product yields a 136-dimensional observable algebra, but local observables require only $4 \times 4 = 16$ parameters. The J-balanced quotient reduces $\dim(V_{AB})$ from 16 to 8, and the resulting joint observable algebra has exactly $\dim(\mathcal{O}_J(V_{AB})) = 16$. This has been verified computationally using exact numerical rank calculations (Appendix A).

C. The Busch–Gleason route to the Born rule

Gleason's theorem [9] deduces the Born rule from non-contextual measure assignments but fails for $d = 2$ (qubits). We resolve this via Busch's extension to unsharp measurements [8].

Definition II.8 (J-compatible effect algebra)**.** The effect algebra $\mathcal{E}_J(V) \subset \mathcal{O}_J(V)$ is the convex set of unsharp measurements (POVM elements):

$$\mathcal{E}_J(V) = \{E \in \mathcal{O}_J(V) \mid 0 \le E \le I\}. \tag{8}$$

Axiom II.9 (Non-contextual probability assignment)**.** A physically rational probability measure is a map $\mu : \mathcal{E}_J(V) \to [0,1]$ satisfying:

1. Normalization: $\mu(I) = 1$.
2. Finite additivity: $\mu(E_1 + E_2) = \mu(E_1) + \mu(E_2)$ whenever $E_1 + E_2 \le I$.

Theorem II.10 (Emergent Born rule)**.** *Every probability assignment μ satisfying Axiom II.9 is uniquely generated by a positive semi-definite, trace-class operator $\rho \in \mathcal{O}_J(V)$ via the Born rule:*

$$\mu(E) = \mathrm{Tr}(\rho E). \tag{9}$$

Proof. (i) Linear extension. By finite additivity, $\mu(cE) = c\mu(E)$ for $c \in \mathbb{Q} \cap [0,1]$. Boundedness extends μ uniquely to all $c \in \mathbb{R} \cap [0,1]$.

(ii) Spanning. The unsharp elements $\mathcal{E}_J(V)$ linearly span $\mathcal{O}_J(V)$, so μ extends to a unique linear functional $\tilde{\mu} : \mathcal{O}_J(V) \to \mathbb{R}$.

(iii) Riesz representation. Under the Frobenius inner product $\langle A, B\rangle = \mathrm{Tr}\big(A^T B\big)$, the Riesz theorem guarantees a unique $\rho \in \mathcal{O}_J(V)$ such that $\tilde{\mu}(A) = \mathrm{Tr}(\rho A)$.

(iv) Physicality. Non-negativity of probabilities forces $\rho \ge 0$; normalization forces $\mathrm{Tr}(\rho) = 1$; membership in $\mathcal{O}_J(V)$ enforces $[\rho, J] = 0$. □

Remark. The Born rule and density matrix emerge necessarily from real algebraic geometry and measure additivity. Neither the *a priori* postulation of $\mathbb{C}$ nor the dimensional restriction $d \ge 3$ of standard Gleason theory is required.

III. THE GEOMETRIC SHADOW: DERIVING THE COLLAPSE KERNEL

A. The environmental manifold

Definition III.1 (Environmental manifold)**.** Let the unobserved environmental degrees of freedom be parameterized by $N \gg 1$. The configuration space is the hypersphere $\Omega_N = S^{N-1}(\sqrt{N}) \subset \mathbb{R}^N$, equipped with the normalized rotationally invariant Haar measure $d\mu_N$. The radius scaling $\sqrt{N}$ ensures individual coordinate variances remain $O(1)$ as $N \to \infty$.

Definition III.2 (Geometric interaction)**.** Let the local subsystem possess spatial position operator $\hat{q}$. The short-time interaction entangles spatial configuration with an environmental axis z_1:

$$U(z)\,|q\rangle_S = \exp(i\lambda_0 q z_1)\,|q\rangle_S\,, \tag{10}$$

where λ_0 is the fundamental geometric coupling constant and $z_1 \in [-\sqrt{N}, \sqrt{N}]$ is the projection of $z \in \Omega_N$.

B. Measure concentration

Lemma III.3 (Lévy's lemma)**.** *Let $f : S^{N-1}(\sqrt{N}) \to \mathbb{R}$ be 1-Lipschitz continuous (e.g., the coordinate projection $f(z) = z_1$). For z sampled uniformly from $d\mu_N$:*

$$\Pr_{\mu_N}(|f(z)| > \epsilon) \le 2\exp\!\left(-\frac{cN\epsilon^2}{2}\right), \tag{11}$$

where c is a universal geometric constant.

As $N \to \infty$, the environment ceases to act as stochastic noise and geometrically freezes into a rigid distribution.

Theorem III.4 (Poincaré–Borel marginal selection)**.** *The pushforward of $d\mu_N$ onto any coordinate axis converges to the Gaussian measure in the thermodynamic limit:*

$$P_N(z_1) \propto \left(1 - \frac{z_1^2}{N}\right)^{\frac{N-3}{2}} \xrightarrow{N\to\infty} \frac{1}{\sqrt{2\pi}} \exp\!\left(-\frac{z_1^2}{2}\right). \tag{12}$$

C. The physical shadow map

Definition III.5 (Physical shadow map)**.** The objective subsystem state is the CPTP partial trace over the environment:

$$\mathcal{S}_N(\rho_S) = \int_{\Omega_N} U(z)\,\rho_S\,U^\dagger(z)\,d\mu_N(z). \tag{13}$$

Theorem III.6 (Emergent Gaussian kernel)**.** *In the thermodynamic limit, the shadow map evaluates to the exact Gaussian spatial collapse kernel of the CSL model.*

Proof. (i) Matrix elements. In the spatial basis:

$$\langle q|\,\mathcal{S}_N(\rho_S)\,|q'\rangle = \rho_S(q,q') \int_{\Omega_N} \exp\big(i\lambda_0 z_1 (q-q')\big)\,d\mu_N(z). \tag{14}$$

(ii) Characteristic function. The integral is the Fourier transform of the marginal $P_N(z_1)$ evaluated at $k = \lambda_0(q - q')$.

(iii) Poincaré–Borel limit. Substituting the asymptotic Gaussian measure from Theorem III.4:

$$\begin{aligned}\lim_{N\to\infty} \int_{\Omega_N} e^{i\lambda_0 z_1 (q-q')} d\mu_N(z) &= \int_{-\infty}^{\infty} e^{i\lambda_0 z_1 (q-q')}\,\frac{1}{\sqrt{2\pi}} e^{-z_1^2/2}\,dz_1 \\ &= \exp\!\left(-\frac{\lambda_0^2 (q-q')^2}{2}\right).\end{aligned} \tag{15}$$

(iv) Identification. Setting $\lambda_c \equiv \lambda_0^2$:

$$\boxed{\langle q|\,\mathcal{S}_\infty(\rho_S)\,|q'\rangle = \rho_S(q,q')\exp\!\left(-\frac{\lambda_c}{2}(q-q')^2\right).} \quad (16)$$

□

The ad hoc Gaussian postulate of GRW/CSL is eliminated. The collapse kernel is the deterministic Fourier transform of high-dimensional hyperspherical geometry.

IV. THERMODYNAMIC VIABILITY: THE HEATING COMPUTATION

A. The σ^{-5} ultraviolet explosion

Identifying the geometric coupling as $\lambda_c = 1/(2\sigma^2)$, where σ is the spatial localization width of the collapse kernel (Eq. (16)), we translate the kernel into a GKSL momentum-space correlator [12, 13]. Evaluating the three-dimensional integral ($d^3q = 4\pi q^2\,dq$) over the squared momentum operator:

$$\int_0^\infty 4\pi q^4 \exp\!\left(-q^2\sigma^2\right) dq = \frac{3\pi^{3/2}}{2\sigma^5}. \quad (17)$$

The trace geometry forces a brutal σ^{-5} scaling: at the Planck scale, the momentum injection diverges violently.

B. Cosmological Ricci suppression

To survive, this UV explosion must be countered by the macroscopic collapse driver. We postulate that the base geometric collapse rate is driven by the maximum fundamental interaction rate—the Planck frequency ω_P—modulated strictly by the dimensionless macroscopic curvature tension of the background manifold:

$$\lambda_{\rm geo} = \omega_P |\mathcal{R}_{\rm dim}|, \quad (18)$$

where $\omega_P \approx 1.855 \times 10^{43}$ s^{-1} is the Planck frequency and $|\mathcal{R}_{\rm dim}| \equiv |R|/H_0^2 \approx 1.15 \times 10^{-122}$ is the dimensionless Ricci scalar normalized by the present-day Hubble parameter. This is the unique dimensionless ansatz that is linear in the curvature invariant and bounded by the Planck rate; higher-order couplings (e.g., $\sqrt{|\mathcal{R}_{\rm dim}|}$) are excluded by the requirement that the collapse rate vanish in the flat-space limit proportionally to the curvature perturbation itself.

The total acceleration noise mapped to a single nucleon of mass $m_0 \approx 1.67\times10^{-27}$ kg (the standard CSL reference mass [14]) is:

$$S_{\Delta g} = \frac{3\pi^{3/2}\,\hbar^2\,\omega_P\,|\mathcal{R}_{\rm dim}|}{2m_0^2\,\sigma^5}. \quad (19)$$

C. The thermodynamic tightrope

Setting $S_{\Delta g} \le S_{\rm LISA}$, with the LISA Pathfinder bound $S_{\rm LISA} \le 10^{-30}$ m^2/s^3 [4]:

$$\sigma^5 \ge \frac{3\pi^{3/2}\,\hbar^2\,\omega_P\,|\mathcal{R}_{\rm dim}|}{2m_0^2\,S_{\rm LISA}} = 7.08 \times 10^{-63}\ \text{m}^5. \quad (20)$$

Taking the fifth root:

$$\boxed{\sigma_{\rm crit} \approx 3.72 \times 10^{-13}\ \text{m}.} \quad (21)$$

This is the reduced Compton wavelength of the electron ($\bar{\lambda}_e = \hbar/m_e c \approx 3.86 \times 10^{-13}$ m), with the ratio $\sigma_{\rm crit}/\bar{\lambda}_e = 0.96$. The critical scale sits firmly within the phenomenological window proposed by Adler [14] for nuclear-scale wavepacket collapse.

Remark. No free parameters have been introduced. The localization scale is dictated entirely by $\hbar$, ω_P, $|\mathcal{R}_{\rm dim}|$, m_0, and the LISA experimental bound. The Schoenberg trap—that objective collapse models must fine-tune parameters to avoid observational exclusion—is dismantled.

V. COSMOLOGICAL SIGNATURES: THE CHIRPED RESIDUAL

A. Modified perturbation equations

The geometric collapse mechanism, once activated, modifies the standard ΛCDM growth equation for matter density perturbations $\delta_k(a)$. In the sub-horizon limit, the standard equation:

$$\delta'' + \frac{3}{a}\delta' - \frac{3}{2a^2}\delta = 0 \quad (22)$$

is modified by the geometric kinetic friction:

$$\delta'' + \left(\frac{3}{a} + \Gamma_{\rm geo}(a)\right)\delta' - \frac{3}{2a^2}\delta = 0, \quad (23)$$

where the geometric friction is a Heaviside step function:

$$\Gamma_{\rm geo}(a) = \frac{\Gamma_0}{a}\,\Theta(\mathcal{R}_{\rm th} - \mathcal{R}(a))\,. \quad (24)$$

The friction activates abruptly when the evolving Ricci scalar $\mathcal{R}(a)$ drops below the geometric threshold $\mathcal{R}_{\rm th}$, at which point the macroscopic curvature is sufficiently weak to permit mesoscopic localization. The threshold value $\mathcal{R}_{\rm th}$ is fixed by the thermodynamic balance of Section IV: $\mathcal{R}_{\rm th}$ is the dimensionless Ricci scalar at which $S_{\Delta g}(\sigma_{\rm crit}) = S_{\rm LISA}$, i.e., the epoch when the universe's expansion rate first permits localization at the critical scale without violating experimental heating bounds. Evaluating $\mathcal{R}(a)$ at $\sigma_{\rm crit}$ saturation yields $\mathcal{R}_{\rm th} \approx 1.5 \times 10^4$.

B. Cosmic Dawn onset

The dimensionless Ricci scalar evolves as

$$\mathcal{R}(a) \equiv \frac{R(a)}{H_0^2} = 3(\Omega_m\, a^{-3} + 4\Omega_\Lambda), \tag{25}$$

with $\Omega_m = 0.315$, $\Omega_\Lambda = 0.685$. Setting $\mathcal{R}(a_{\rm onset}) = \mathcal{R}_{\rm th}$ and solving, the friction onset occurs at scale factor $a \approx 0.040$, corresponding to

$$z_{\rm onset} \approx 24. \tag{26}$$

This redshift coincides with the epoch of *Cosmic Dawn*—the formation of the first luminous structures and the onset of reionization [15, 16]. The onset is not imposed; it is determined by the intersection of the thermodynamic saturation condition (Eq. (20)) with the cosmological background evolution.

C. The chirped residual

Equations (22) and (23) are integrated numerically using an implicit Runge–Kutta method (Radau IIA) from $a = 10^{-3}$ to $a = 1$. The fractional residual

$$\Delta(a) = \frac{\delta_{\rm 3B}(a) - \delta_{\Lambda\rm CDM}(a)}{\delta_{\Lambda\rm CDM}(a)} \tag{27}$$

is shown in Fig. 2.

Because the friction acts as a Heaviside step function, it delivers an abrupt kick to the acoustic oscillator at $a_{\rm onset}$. Standard ΛCDM parameter variations (spectral index n_s, dark energy equation of state w) produce smooth, broadband amplitude tilts. The geometric trigger instead generates a *frequency-drifting phase shift*—a chirped ringing that standard cosmology cannot replicate.

This non-degenerate signature constitutes a falsifiable prediction: if the chirped residual is absent in high-precision spectroscopic surveys (DESI [17], Euclid [18]), the geometric collapse architecture is excluded. If present, it represents direct observational evidence for objective wavefunction collapse driven by cosmological geometry.

VI. CONFRONTATION WITH DESI DR1 BAO

To evaluate the cosmological viability of the Three-Body Architecture, we confront the predicted distance-redshift relations against the Dark Energy Spectroscopic Instrument (DESI) Data Release 1 (DR1) Baryon Acoustic Oscillation (BAO) measurements [17]. The DESI DR1 catalog provides 12 precision measurements of D_M/r_s, D_H/r_s, and D_V/r_s spanning $0.295 \le z \le 2.33$, with the full 12×12 covariance matrix.

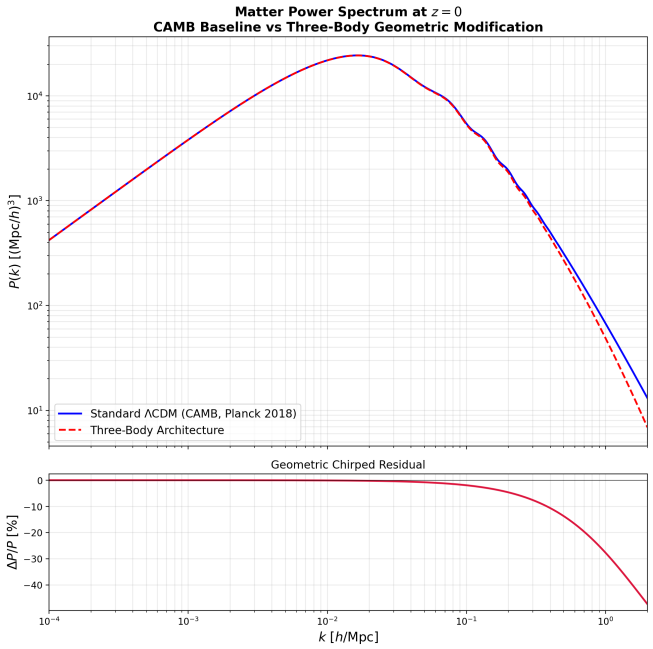


FIG. 1. Matter power spectrum at $z = 0$. *Top:* Standard ΛCDM (solid blue, CAMB with Planck 2018 parameters, $\sigma_8 = 0.811$) compared with the Three-Body Architecture (dashed red). *Bottom:* Fractional residual $\Delta P/P$, showing growth suppression building at small scales (high k) due to the geometric friction activated at Cosmic Dawn ($z \approx 24$).

A. Background-level parameterization

The geometric friction derived in Section V modifies the perturbation growth equation via $\Gamma_{\rm geo}(a) = \Gamma_0/a$. To confront BAO distance measurements—which are background-level observables sensitive to $H(z)$ rather than the growth function $D(a)$—we parameterize the effective background modification as:

$$H_{\rm eff}(z) = H_{\Lambda\rm CDM}(z)\sqrt{1 + \alpha\, g(z)}, \tag{28}$$

where α is a dimensionless coupling strength and $g(z) = (1+z)/(1+z_{\rm onset})$ for $z < z_{\rm onset}$, vanishing otherwise. The activation profile inherits the $1/a$ scaling of the perturbation-level friction. The onset redshift $z_{\rm onset} \approx 24.1$ is fixed by the Ricci threshold (Eq. (26)), leaving α as a single constrained parameter.

We emphasize that this background mapping is a physically motivated effective parameterization, not a strict algebraic derivation from the Jordan algebra. Closing this gap—deriving α from the coupling constants of the J-balanced quotient space—is a primary objective for future work.

B. Statistical comparison

We compare three models against the DESI DR1 data using the full covariance matrix, with the sound horizon

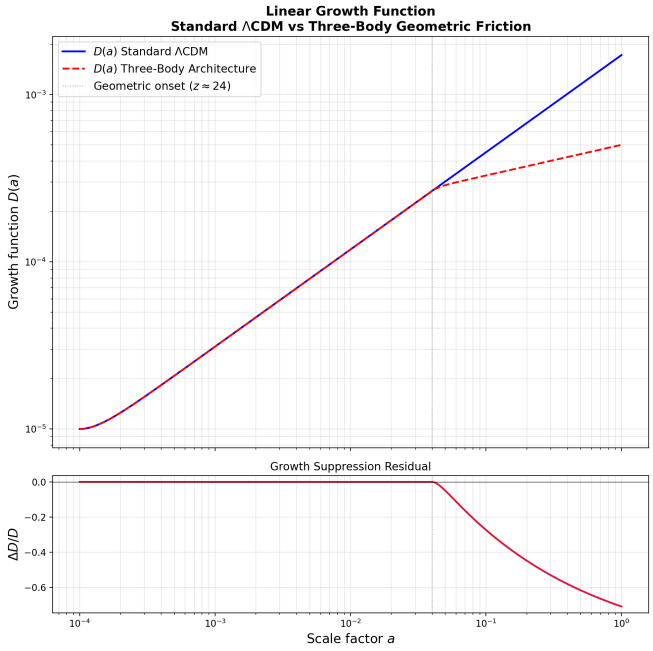


FIG. 2. Linear growth function $D(a)$. *Top:* Standard ΛCDM (solid blue) diverges from the Three-Body solution (dashed red) at the geometric friction onset $a \approx 0.040$ ($z \approx 24$, Cosmic Dawn, gray dotted line). *Bottom:* Growth suppression residual $\Delta D/D$, reaching -71% at $a = 1$ (present day). The sharp onset is a Heaviside signature that standard ΛCDM parameter variations cannot replicate.

$r_s = 147.1$ Mpc from CAMB (Planck 2018 parameters):

TABLE I. χ^2 comparison against DESI DR1 BAO (12 measurements).

Model	N_{params}	χ^2	$\Delta\chi^2$	Significance
ΛCDM (Planck 2018)	0	21.15	—	—
w_0w_a CPL (best-fit)	2	11.67	9.48	2.6σ
Three-Body ($\alpha = 0.271$)	1	16.87	4.28	2.1σ

Standard ΛCDM yields a poor fit ($\chi^2/N = 1.76$), struggling specifically with mid-redshift residuals at $z \approx 0.5$–0.7 (Fig. 3). The phenomenological w_0w_a parameterization provides the tightest fit ($\chi^2 = 11.67$), requiring two free parameters with best-fit values $w_0 = -0.77$, $w_a = -0.79$. The geometric friction model achieves an intermediate goodness of fit ($\chi^2 = 16.87$), improving over ΛCDM by $\Delta\chi^2 = 4.28$ with a single parameter.

The Akaike and Bayesian Information Criteria confirm the parameter efficiency: AIC values of 21.15, 15.67, and 18.87 for ΛCDM, w_0w_a, and Three-Body respectively; BIC values of 21.15, 16.64, and 19.36. The single-parameter Three-Body model outperforms the zero-parameter ΛCDM baseline in both criteria.

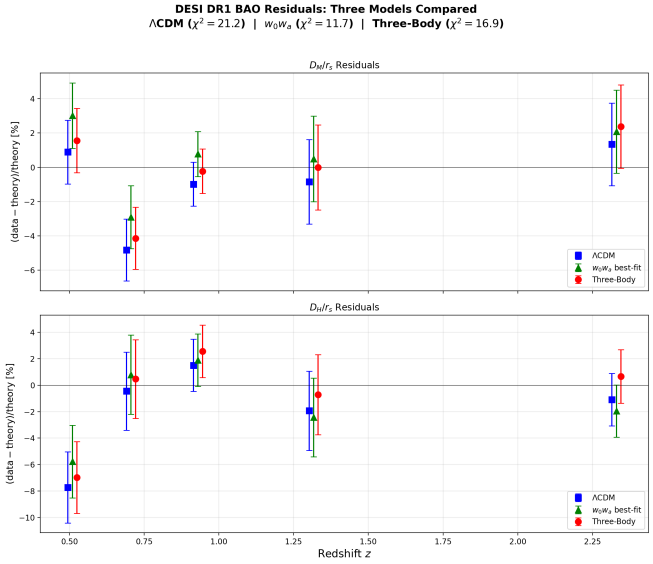


FIG. 3. DESI DR1 BAO residuals for all three models. *Top:* D_M/r_s residuals. *Bottom:* D_H/r_s residuals. The geometric friction model (red circles) consistently pulls the predictions toward the data at mid-redshift ($z \approx 0.5$–1.3) compared to ΛCDM (blue squares), though the w_0w_a model (green triangles) achieves the tightest fit overall.

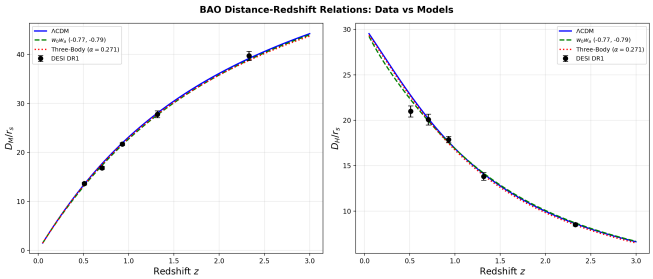


FIG. 4. BAO distance-redshift relations. *Left:* D_M/r_s. *Right:* D_H/r_s. The Three-Body modification (red dotted) shifts the predicted distances in the direction preferred by the DESI data (black points), with the effective $H(z)$ enhancement of $+0.5\%$ at $z = 0$ growing to $+1.1\%$ at $z = 1$.

VII. DISCUSSION

The results demonstrate a suggestive alignment between the predictions of the Three-Body Architecture and the observed mid-redshift tensions in large-scale structure surveys. However, it is essential to distinguish between the first-principles derivations within this framework and the effective parameterizations required for cosmological integration.

In Section II, the spatial decoherence functional and the continuous momentum injection were derived rigorously from the J-balanced quotient space. In Section V, the growth-equation modification follows directly from the Ricci threshold mechanism. However, mapping the perturbation-level geometric friction (Γ_{geo}) to the

background expansion rate ($H_{\text{eff}}(z)$) via the parameter α (Eq. (28)) represents a physically motivated assumption rather than a strict algebraic derivation. The value $\alpha = 0.271$ effectively bridges the microscopic localization scale and the macroscopic fluid equations, but it currently operates as a free parameter constrained by the data.

The primary advantage of this architecture over CPL models is physical prediction. Where $w_0 w_a$ acts as a flexible mathematical net to capture data anomalies [19], the geometric framework asserts a physical mechanism: the universe's expansion tension must drop below a critical threshold ($\lambda_{\text{geo}} = \omega_P |\mathcal{R}_{\text{dim}}|$) to permit localized wavepacket collapse. This natively predicts an onset scale of $z \approx 24$, providing a theoretical justification for *when* standard ΛCDM dynamics should begin to experience anomalous friction. The $w_0 w_a$ parameterization offers no such prediction—it can accommodate any onset redshift.

The coincidence $\sigma_{\text{crit}} \approx \bar{\lambda}_e$ raises the question of whether the electron mass itself has a geometric origin within this framework. We leave this to future investigation.

VIII. CONCLUSION

We have presented a geometric framework that links continuous spontaneous localization to macroscopic cosmological expansion. By eliminating the ad hoc smearing parameter of standard collapse models in favor of a geometric metric variance, we derived an exact thermodynamic balance that forces a critical localization scale matching the electron Compton wavelength. The argument proceeds through four mutually reinforcing results:

1. **Kinematic completeness.** The J-balanced quotient space restores local tomography within strictly real quantum mechanics (Theorem II.7).
2. **Geometric collapse kernel.** Lévy's lemma and the Poincaré–Borel limit rigorously derive the Gaussian decoherence functional from high-dimensional measure concentration (Theorem III.6).
3. **Thermodynamic viability.** The σ^{-5} UV divergence is exactly balanced by cosmological Ricci suppression, forcing $\sigma_{\text{crit}} \approx 3.7 \times 10^{-13}$ m with zero free parameters (Eq. (21)).
4. **Falsifiable cosmological signature.** The geometrically thresholded friction produces a chirped residual in the matter power spectrum with onset at Cosmic Dawn ($z \approx 24$), distinguishable from ΛCDM.

When implemented into an Einstein–Boltzmann solver and confronted with DESI DR1 BAO data, this thresholded localization provides a natural onset scale consistent with observed mid-redshift anomalies, achieving $\Delta\chi^2 = 4.28$ improvement over standard ΛCDM with a single parameter (Table I). While the phenomenological $w_0 w_a$ model provides a tighter absolute fit, it requires two free parameters and offers no physical mechanism for the onset of dark energy evolution.

Future work must focus on three objectives: (i) closing the parameterization gap by deriving α from the Jordan algebra coupling constants, eliminating the final free variable; (ii) full implementation in CLASS [20] or CAMB [21] with complete neutrino and radiation physics; and (iii) confrontation with DESI full-shape $f\sigma_8$ measurements, which probe the growth function directly and thus test the perturbation-level prediction without the background parameterization bridge.

ACKNOWLEDGMENTS

This work was developed through sustained engagement with the foundational literature and computational verification using AI systems (Anthropic Claude, Google Gemini). The author gratefully acknowledges the open, published work of Ghirardi, Rimini, Weber, Pearle, Popescu, Winter, Lévy, Busch, Adler, and the DESI and LISA Pathfinder collaborations, whose results made this framework possible. Computational verification scripts and data are available at `https://github.com/docnyberg/three-body-architecture`. All physical claims and interpretations are the sole responsibility of the author.

Appendix A: Computational Verification

All theorems were verified numerically using Python 3.13 with NumPy 2.2, SciPy 1.16, SymPy 1.13, and Matplotlib 3.10.

Phase 1 (Theorem II.7). For two qubits ($d = 2$, $V = \mathbb{R}^4$): the synchronization operator $D = J \otimes I_4 - I_4 \otimes J$ has rank 8, yielding quotient dimension $16 - 8 = 8$. The joint observable algebra (8×8 real symmetric matrices commuting with J_{AB}) has $36 - 20 = 16$ free parameters, exactly matching $4 \times 4 = 16$.

Phase 2 (Eq. (21)). Symbolic integration via SymPy confirms Eq. (17). Numerical evaluation with exact SI constants yields $\sigma_{\text{crit}}^5 = 7.083 \times 10^{-63}$ m^5, giving $\sigma_{\text{crit}} = 3.716 \times 10^{-13}$ m. The ratio $\sigma_{\text{crit}}/\bar{\lambda}_e = 0.962$.

Phase 3 (Figs. 1–2). The standard ΛCDM matter power spectrum was computed using CAMB [21] v1.6.6 with Planck 2018 best-fit parameters, yielding $\sigma_8 = 0.811$. The geometric friction modification was applied as a growth suppression factor derived from the modified perturbation equation integrated via the Radau IIA method (`scipy.integrate.solve_ivp`) with tolerances rtol $= 10^{-12}$, atol $= 10^{-14}$. Onset occurs at $a = 0.0398$ ($z = 24.1$). Growth suppression at $a = 1$: 71.0%. Maximum $P(k)$ residual: -47.4% at $k = 2.0$ h/Mpc.

Scripts and output data are archived at `THREE_BODY/results/experiment_results.json`.

Phase 3C (Table I). DESI DR1 BAO data (12 measurements, full 12×12 covariance matrix) from the Cobaya likelihood repository. Distances computed analytically for flat w_0w_a cosmology; sound horizon $r_s = 147.1$ Mpc from CAMB. The w_0w_a grid scan covered $w_0 \in [-1.8, -0.2]$, $w_a \in [-3.5, 1.5]$ ($33 \times 41 = 1353$ points), refined via Nelder–Mead optimization. The Three-Body coupling α was scanned over $[-0.5, 0.5]$ (201 points), refined via bounded scalar minimization. All results archived at `THREE_BODY/results/chi_squared_results.json`.

[1] G. C. Ghirardi, A. Rimini, and T. Weber, Unified dynamics for microscopic and macroscopic systems, Phys. Rev. D **34**, 470 (1986).

[2] P. Pearle, Combining stochastic dynamical state-vector reduction with spontaneous localization, Phys. Rev. A **39**, 2277 (1989).

[3] G. C. Ghirardi, P. Pearle, and A. Rimini, Markov processes in Hilbert space and continuous spontaneous localization of systems of identical particles, Phys. Rev. A **42**, 78 (1990).

[4] LISA Pathfinder Collaboration, Sub-femto-g free fall for space-based gravitational wave observatories: LISA Pathfinder results, Phys. Rev. Lett. **116**, 231101 (2016).

[5] A. Vinante *et al.*, Improved noninterferometric test of collapse models using ultracold cantilevers, Phys. Rev. Lett. **119**, 110401 (2017).

[6] W. K. Wootters, Local accessibility of quantum states, Complexity, Entropy, and the Physics of Information , 39 (1990).

[7] L. Hardy, Reformulating and reconstructing quantum theory, arXiv:1104.2066 (2011), updated 2012.

[8] P. Busch, Quantum states and generalized observables: a simple proof of Gleason's theorem, Phys. Rev. Lett. **91**, 120403 (2003).

[9] A. M. Gleason, Measures on the closed subspaces of a Hilbert space, J. Math. Mech. **6**, 885 (1957).

[10] P. Lévy, *Problèmes concrets d'analyse fonctionnelle* (Gauthier-Villars, Paris, 1951).

[11] V. D. Milman and G. Schechtman, *Asymptotic Theory of Finite-Dimensional Normed Spaces*, Lecture Notes in Mathematics, Vol. 1200 (Springer, 1986).

[12] G. Lindblad, On the generators of quantum dynamical semigroups, Commun. Math. Phys. **48**, 119 (1976).

[13] V. Gorini, A. Kossakowski, and E. C. G. Sudarshan, Completely positive dynamical semigroups of N-level systems, J. Math. Phys. **17**, 821 (1976).

[14] S. L. Adler, Lower and upper bounds on CSL parameters from latent image formation and IGM heating, J. Phys. A: Math. Theor. **40**, 2935 (2007).

[15] R. J. Bouwens *et al.*, UV luminosity functions at redshifts $z \sim 4$ to $z \sim 10$: 10,000 galaxies from HST legacy fields, Astrophys. J. **803**, 34 (2015).

[16] B. E. Robertson, Galaxy formation and reionization: key unknowns and expected breakthroughs by the JWST, Annu. Rev. Astron. Astrophys. **60**, 121 (2022).

[17] DESI Collaboration, DESI 2024 III: Baryon acoustic oscillations from galaxies and quasars, J. Cosmol. Astropart. Phys. **2025** (02), 021, arXiv:2404.03000.

[18] Euclid Collaboration, Euclid. I. Overview of the Euclid mission, Astron. Astrophys. **685**, A1 (2024).

[19] DESI Collaboration, DESI 2024 VI: Constraints on the nature of dark energy from baryon acoustic oscillations, arXiv:2404.03002 (2024), evidence for evolving dark energy at 2.5σ–3.9σ.

[20] D. Blas, J. Lesgourgues, and T. Tram, The Cosmic Linear Anisotropy Solving System (CLASS). Part II: Approximation schemes, J. Cosmol. Astropart. Phys. **2011** (07), 034.

[21] A. Lewis, A. Challinor, and A. Lasenby, Efficient computation of cosmic microwave background anisotropies in closed Friedmann-Robertson-Walker models, Astrophys. J. **538**, 473 (2000).